Available online at www.sciencedirect.com
SCIENCE DIRECT®
Journal of Computational Physics 211 (2006) 262–288
JOURNAL OF COMPUTATIONAL PHYSICS
www.elsevier.com/locate/jcp

Modal reduction of mathematical models of biological molecules

Aiqin Li, Earl H. Dowell *

Department of Mechanical Engineering and Materials Science, Duke University, 144 Hudson Hall, P.O. Box 90302, Durham, NC 27708-0300, United States

Received 14 January 2005; received in revised form 8 April 2005; accepted 24 May 2005
Available online 14 July 2005

Abstract

This paper reports a detailed study of modal reduction based on either linear normal mode (LNM) analysis or proper orthogonal decomposition (POD) for modeling a single α-D-glucopyranose monomer as well as a chain of monomers attached to a moving atomic force microscope (AFM) under harmonic excitations. Also a modal reduction method combining POD and component modal synthesis is developed. The accuracy and efficiency of these methods are reported. The focus of this study is to determine to what extent these methods can reduce the time and cost of molecular modeling and simultaneously provide the required accuracy. It has been demonstrated that a linear reduced order model is valid for small amplitude excitation and low frequency excitation. It is found that a nonlinear reduced order model based on POD modes provides a good approximation even for large excitation while the nonlinear reduced order model using linear eigenmodes as the basis vectors is less effective for modeling molecules with a strong nonlinearity. The reduced order model based on component modal synthesis using POD modes for each component also gives a good approximation. With the reduction in the dimension of the system using these methods the computational time and cost can be reduced significantly.

Keywords: Modal reduction; Biological molecules; Linear normal mode; Proper orthogonal decomposition; Component modal analysis

1. Introduction

Biomolecular motions involve a large number of atoms and take place over a great range of time and length scales. Moreover, because of the existence of high frequency motions, the usual time step in a

* Corresponding author. Tel.: +1 919 660 5321; fax: +1 919 660 0089.
E-mail addresses: aiqin.li@duke.edu (A. Li), dowell@ee.duke.edu (E.H. Dowell).

0021-9991/$ - see front matter © 2005 Elsevier Inc. All rights reserved.
doi:10.1016/j.jcp.2005.05.021

molecular dynamics simulation is around 10^{-15} s. These characteristics make a numerical molecular dynamic simulation a computationally intensive task. There is a clear need to reduce the cost of the computation. So far several schemes have been developed to accomplish this goal. One way is to reduce the time and cost for the evaluation of non-bonded forces, electrostatics forces and van der Waals forces. Since van der Waals interactions are short ranged, their calculation can be restricted to neighboring pairs. For electrostatic forces several algorithms have been proposed such as Ewald summation [1], particle–particle/particle mesh (PPPM) method [2] and fast multipole algorithms (FMAs) [3]. Also in the widely used computer code, CHARMM [4], a cut-off is used to exclude from the force calculation those atom pairs with a distance greater than the cut-off distance. Another approach being used is to make full use of high performance software techniques. Several computer programs such as NAMD [5] and EGO [6] are designed to run simulations on parallel computers.

An alternative approach is modal reduction as presented in this paper. The premise that motivates modal reduction is that complex systems can have a relatively simple dynamic behavior which only depends on a relatively small number of essential variables. The challenge for constructing low-dimensional models for complex physical systems is the choice of basis vectors. Various basis vectors for the subspace have been proposed.

As far as linear systems are concerned, the most common method is linear normal mode (LNM) or eigenmode analysis. Modal reduction is well established for linear dynamic systems since the linear systems have the property of superposition.

By contrast, modal reduction for nonlinear systems is much more complicated. Generally linear normal modes are no longer invariant manifolds in nonlinear vibration systems. However, it is valid to simulate small fluctuations by assuming the potential energy is harmonic in the neighborhood of equilibrium states (conformations) based on linear normal modes. The interested reader is referred to [7] for a discussion of existing methods. For the basic methodology used in biological systems, see Ref. [8]. It is known that the reduced order models for nonlinear systems that are based on the linear eigenmode space can give qualitatively wrong results due to the contamination from the non-modeled modes. More specifically, it has been observed that projecting nonlinear equations onto linear eigenmodes predicts incorrect hardening and softening regions of the potential energy. See [9] and the references therein for examples. To overcome this problem, several invariant manifolds such as center manifolds [10], inertial manifolds and nonlinear normal modes (NNMs)[11] have been proposed. But these approaches are still under development and have been primarily used for low-dimensional or relatively simple systems [12–15]. For complex and high-dimensional systems these methods are often computationally intractable. Another method that has received attention recently is the proper orthogonal decomposition method (POD) also known as the Karhunen–Loeve (K–L) method or principal modal analysis (PCA).

The POD method is a procedure for extracting the essential information from a set of data obtained in experiments or numerical simulations, thus providing a optimal basis for modal reduction. For a physical interpretation of POD modes (POM), see [16–18] for detailed discussions. It has been proven that POM are actually the linear modes of vibration for linear symmetric undamped free-vibration systems with an identity mass matrix [16]. In addition to being optimal in a least square sense, the POD method has the advantage that POM are completely data dependent and do not need any prior knowledge of the system. Hence, this procedure is powerful in generating low-dimensional models for complex systems described by a high-dimensional discrete system or a continuous system. Compared with other nonlinear invariant manifold reduction methods, POD modes are much easier to compute. Because of these properties the POD method is widely used in various fields such as data analysis, image processing, and modal reduction. One of the earliest applications of POD may be traced back to turbulence modeling by Lumey in 1967 [19]. Now POD is emerging as a useful tool in structural dynamics and time-dependent fluid dynamics. It has been used to build reduced order models in a variety of contexts [20–23].

The application of modal analysis to molecular dynamics first appeared in the early 1980s. In [24], the author shows that multiple minima exist in proteins and the harmonic approximation of the potential

energy is in question. Paradoxically, in [25] it is proven that the very low-frequency normal modes make the major contributions to the conformational fluctuations at thermal equilibrium and the author argued that this fact justifies the use of variables of very-low-frequency normal modes to describe significant conformational dynamics of proteins. The use of traditional normal modes is still under study today. Moreover, modal analysis of a biopolymer is still interesting since it does provide physical insight in some cases. As an alternative to traditional normal modal analysis, POD has been introduced in molecular dynamics. In different publications in the literature, it carries different names: collective coordinates, quasi-harmonic analysis, principal component analysis. In [26], the authors applied both normal modal analysis and principal component analysis to the dynamics of BPTI and the results show that the first principal component makes an overwhelmingly large contribution to the total mean-square fluctuation and represents the transitions between minima. For more examples, see references [27–31]. The results of these papers support the use of modal reduction in computational biology.

However, so far in molecular dynamics most reduced order models using normal modes or POD are assumed to be linear around the static equilibrium state or conformation. The study of a nonlinear reduced order model is rarely considered. In this paper, normal modes and POD modes are used to construct linear and nonlinear reduced order models for a α-D-glucopyranose monomer to determine if modal reduction can provide a good approximation to the original system and can improve the efficiency of computation in molecular dynamics. This is a continuation of our previous studies that were mainly on linear models [32].

In addition, a reduced order model based on POD and component modal synthesis (CMS) is also constructed. As is well known, component modal synthesis can be advantageous in modeling large systems. For biological molecules, the dimension of the system is very high. The calculation of POM for the entire system is very expensive since the correlation matrix is so big. And also the accuracy may be in doubt when solving a large eigenvalue problem. Thus, CMS is introduced here. To demonstrate the utility of this method, the simulation of a ten-monomer amylose chain is carried out.

2. Methods

The chemical formula of α-D-glucopyranose is $C_6H_{12}O_6$. It includes 24 atoms and has a six-member ring structure with one side-group. The semi-empirical potential energy method is used in the simulation. To date several kinds of potential functions have been proposed for this method such as the Amber force field and the CHARMM force field. Each field has been improved several times. For example, the earliest version of the CHARMM force field has been improved in 1988 [33], in 1995 and in 2001 [34]. In this paper, the latest version is used.

2.1. Nonlinear dynamic equations of motion

The schematic diagram of a α-D-glucopyranose chain with an atomic force microscope (AFM) attached is shown in Fig. 1.

The potential energy of the molecule has the following form:

$$V_{\mathrm{T}} = \sum_{\text{bonds}} k_b(b-b_0)^2 + \sum_{\text{angles}} k_\theta(\theta-\theta_0)^2 + \sum_{\text{torsions}} k_\phi[1+\cos(n\phi-\delta)] + \sum_{i<j}\left(\frac{A_{ij}}{r_{ij}^{12}} - \frac{B_{ij}}{r_{ij}^{6}} + K_{\mathrm{coul}}\frac{e_i e_j}{\epsilon r_{ij}}\right), \tag{1}$$

where the values of b_0 are the equilibrium bond lengths, those of θ_0 are the equilibrium bond angles, n is a periodicity number, δ is a phase factor, r_{ij} is the distance between atom i and atom j, q_i and q_j are atomic partial charges and k_b, k_θ, k_ϕ and K_{coul} are the force parameters.

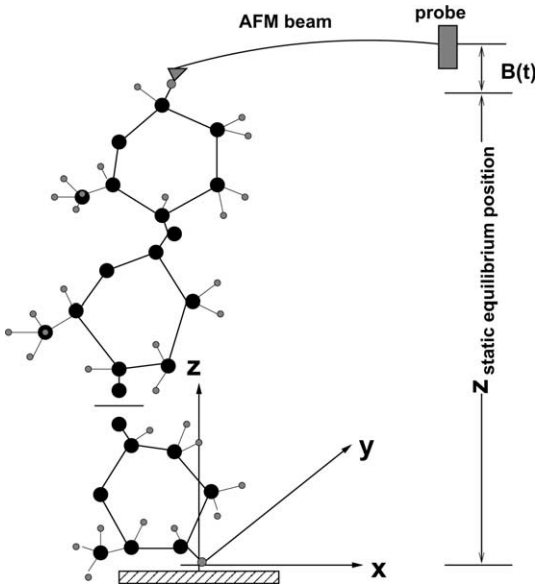

Fig. 1. Schematic diagram for stretching of the molecule by an AFM.

Assume the AFM is attached to atom k and moves along the z-direction. Given the expression for the potential energy and the virtual work in Lagrange's equations for the system, the equations of motion are as follows:

$$\begin{cases} m_i\ddot{\mathbf{r}}_i + \nabla_i(V_\mathrm{T}) = 0, \quad i = 1,2,\ldots,N, \text{ and } i \neq k, \\ m_k\ddot{z}_k + \frac{\partial V_\mathrm{T}}{\partial z_k} - k_\mathrm{s}(B(t) + z_s - z_k) = 0, \end{cases} \tag{2}$$

where N is the total number of atoms, m_i and m_k are the masses of atom i and atom k, $B(t)$ is the excitation displacement prescribed for the AFM base, the vector $\mathbf{r}_i$ is the position vector of atom i as

$$\mathbf{r}_i = x_i\vec{i} + y_i\vec{j} + z_i\vec{k}$$

and k_s is the stiffness of the AFM.

Let $\{x\} = \{x_1, y_1, z_1, x_2, y_2, z_2, \ldots, x_{k-1}, y_{k-1}, z_{k-1}, x_{k+1}, y_{k+1}, z_{k+1}, \ldots, x_N, y_N, z_N\}^\mathrm{T}$. Then the matrix form of Eq. (2) is expressed as,

$$[M]\{\ddot{x}\} - \{F_\mathrm{N}\} + \{F_\mathrm{e}\} = \{k_\mathrm{s}B(t)\delta(i-k)\}, \tag{3}$$

where $[M]$ is a diagonal matrix of the atomic mass, $\{F_\mathrm{e}\}$ is the force due to the AFM and takes the form of $\{F_\mathrm{e}\} = \{k_\mathrm{s}(z_k - z_s)\delta(i-k)\}$, where z_s is the position of the tip of the AFM at force free state and δ is a Delta function, for example, $\delta(i-k) = 0$ when $i \neq k$ and $\delta(i-k) = 1$ when $i = k$. And $\{F_\mathrm{N}\}$ is the force due to atom interactions and is given as

$$f_i = -\frac{\partial V_\mathrm{T}}{\partial x_i}, \quad i = 1,2,\ldots,NN, \tag{4}$$

where NN is the total number of degrees of freedom.

For the present model, a viscous damping force, $\{f_\mathrm{viscous}\}$, is added to Eq. (3) that is assumed to be of the form

$$\mathbf{f}_{i,\mathrm{viscous}} = 2\xi m_i\omega_1\dot{\mathbf{r}}_i,$$

where ω_1 is the fundamental natural frequency. The basic modal damping ratio is taken to be $\xi = 0.1$ in the simulations. The damping matrix is approximately expressed as

$$[C] = 2\xi\omega_1[M].$$

Finally, a compact matrix equation to determine $\{x\}$ can be expressed as,

$$[M]\{\ddot{x}\} + [C]\{\dot{x}\} - \{F_N\} + \{F_e\} = \{k_s B(t)\delta(i-k)\}. \tag{5}$$

2.2. Linear perturbation equations

Based on the nonlinear dynamic equations of motion, a linearized equation for small fluctuations around the static equilibrium position or conformation is considered. Let

$$\{x\} = \{x_s\} + \{\hat{x}\}, \tag{6}$$

where $\{x_s\}$ is the static equilibrium positions and $\{\hat{x}\}$ is a small dynamic fluctuation.

The static equilibrium position, $\{x_s\}$, is determined by

$$\{F_N\} = 0$$

and also the AFM is force free at this state.

Substituting Eq. (6) into Eq. (5) and using a Taylor Series, the linear dynamic perturbation equations for the small motions about the static equilibrium positions are given by

$$[M]\{\ddot{\hat{x}}\} + [C]\{\dot{\hat{x}}\} + [K]\{\hat{x}\} = \{k_s B(t)\delta(i-k)\}, \tag{7}$$

where $[K]$ is a Jacobian matrix about the static equilibrium positions, and the linearized stiffness element K_{ij} is given by

$$K_{ij} = -\left.\frac{\partial f_i}{\partial x_j}\right|_{x_s} + k_s\delta(i-(3k-2))\delta(j-(3k-2)) = \left.\frac{\partial V_T}{\partial x_i \partial x_j}\right|_{x_s} + k_s\delta(i-(3k-2))\delta(j-(3k-2)).$$

For detailed information about the stiffness matrix, K_{ij}, in the Jacobian matrix, see Appendix A in [32].

2.3. Linear normal modes-based reduced order modeling

2.3.1. LNM-based linear reduced order model

Define the reduced modal coordinates as a vector $\{q\}$. The transformation between $\{\hat{x}\}$ and $\{q\}$ is given as

$$\{\hat{x}\} = [\Phi]\{q\}, \tag{8}$$

where $[\Phi]$ is a matrix with eigenvectors as columns and satisfies

$$[\Phi]^T[M][\Phi] = [I]$$

and

$$[\Phi]^T[K][\Phi] = \mathrm{diag}(\omega_i^2) = [\omega^2],$$

where ω_i^2 are eigenvalues of stiffness matrix $[K]$ and mass matrix $[M]$ in increasing order.

Substituting Eq. (8) into Eq. (7), the reduced linear perturbation model is

$$\{\ddot{q}\} + [R]\{\dot{q}\} + [\omega^2]\{q\} = [\Phi]^T\{k_s B(t)\delta(i-k)\}, \tag{9}$$

where

$$[R] = [\Phi]^T[C][\Phi] = 2\xi\omega_1[I].$$

As described in [23,35,36], a quasi-static correction for the linear reduced order model may provide a very effective method to reduce the number of modes that need to be retained for a given level of accuracy. To that end, let

$$\{\hat{x}\} = \{\hat{x}_{Qs}\} + \{\hat{\hat{x}}\}, \tag{10}$$

where $\hat{x}_{Qs}$ is the quasi-static correction (QSC) and $\hat{\hat{x}}$ is an additional small dynamic response. The quasi-static response is defined to be that when the inertia terms, $\ddot{\hat{x}}$ and damping terms, $\dot{\hat{x}}$, are neglected. From Eqs. (7) and (10), thus we have

$$\{\hat{x}_{Qs}\} = [K]^{-1}\{k_s B(t)\delta(i-k)\} \tag{11}$$

and

$$[M]\{\ddot{\hat{\hat{x}}}\} + [C]\{\dot{\hat{\hat{x}}}\} + [K]\{\hat{\hat{x}}\} = -[M]\{\ddot{\hat{x}}_{Qs}\} - [C]\{\dot{\hat{x}}_{Qs}\}. \tag{12}$$

Using the same procedure as before, the linear reduced order dynamic model with a quasi-static correction is given as

$$\{\ddot{q}\} + [R]\{\dot{q}\} + [\omega^2]\{q\} = -\{\mathscr{F}\}, \tag{13}$$

where $\{\mathscr{F}\}$ is a linear force vector that depends upon the quasi-static response of $\hat{x}_{Qs}$.

2.3.2. LNM-based nonlinear reduced order model without quasi-static correction (QSC)

The construction of nonlinear reduced order model is similar to the procedure for linear reduced order model. The solution has the same form of Eqs. (6) and (8), but $\hat{x}$ is not necessarily small in nonlinear reduced order model.

Substituting Eqs. (6) and (8) into Eq. (5), nonlinear ROM without QSC is expressed by

$$\{\ddot{q}\} + [R]\{\dot{q}\} - [\Phi]^{T}\{F_N\} + [\Phi]^{T}\{F_e\} = [\Phi]^{T}\{k_s B(t)\delta(i-k)\}. \tag{14}$$

2.3.3. LNM-based nonlinear reduced order model with QSC

Let

$$\{x\} = \{x_{linear}\} + \{\Delta x\}, \tag{15}$$

where x_{linear} is the linearized static and dynamic response obtained from the linear reduced order model with a quasi-static correction (Eq. (13)). The definition of $\{x_{linear}\}$ is

$$\{x_{linear}\} \equiv \{x_s\} + \{\hat{x}_{Qs}\} + \{\hat{\hat{x}}\},$$

where $\{x_s\}$, $\{\hat{x}_{Qs}\}$ and $\{\hat{\hat{x}}\}$ are the static equilibrium position, the quasi-static response and small dynamic response in the linearized system. However, note that $\{\Delta x\}$ is not necessarily small.

Substituting Eq. (15) into Eq. (5) and using Eqs. (11), (12), one obtains a nonlinear equation in matrix form

$$[M]\{\Delta\ddot{x}\} + [C]\{\Delta\dot{x}\} + \{\Delta F_e\} - \{F_N\} = \{F_{linear}\}, \tag{16}$$

where $\{\Delta F_e\} = \{k_s \Delta x \delta(i-k)\}$ and the linearized force matrix, $\{F_{linear}\}$, is defined by

$$\{F_{linear}\} = [K]\{(\hat{x}_{Qs} + \hat{\hat{x}})\} - \{F_{es}\}$$

where $\{F_{es}\} = \{k_s(x_{linear} - x_s)\delta(i-k)\}$.

Let

$$\{\Delta x\} = [\Phi]\{a\}, \tag{17}$$

$$\{\hat{\hat{x}}\} = [\Phi]\{q\}. \tag{18}$$

Then the corresponding nonlinear reduced order model with the linearized quasi-static correction is given by

$$\{\ddot{a}\} + [R]\{\dot{a}\} + [\Phi]^{\mathrm{T}}\{\Delta F_{\mathrm{e}}\} - [\Phi]^{\mathrm{T}}\{F_{\mathrm{N}}\} = [\Phi]^{\mathrm{T}}\{F_{\mathrm{linear}}\}. \tag{19}$$

Once $\{a\}$, $\{\hat{x}_{\mathrm{Qs}}\}$ and $\{q\}$ are determined from Eqs. (19), (11) and (13), $\{x\}$ can be determined from Eq. (15). Note that when performing the time integration of Eq. (19), one must calculate Eq. (15) at each time step and then determine the nonlinear force vector, $\{F_{\mathrm{N}}\}$.

2.4. Proper orthogonal decomposition modes-based reduced order modeling

From a numerical simulation using Eq. (5), the time histories of the coordinates which determine the positions of all atoms are saved. Then these data are placed in a data matrix Q as

$$[Q]_{NN\times J} = \begin{bmatrix} x^1(1) & \dots & x^1(j) & \dots & x^1(J) \\ \vdots & \vdots & \vdots & \vdots & \vdots \\ x^i(1) & \dots & x^i(j) & \dots & x^i(J) \\ \vdots & \vdots & \vdots & \vdots & \vdots \\ x^{NN}(1) & \dots & x^{NN}(j) & \dots & x^{NN}(J) \end{bmatrix}, \quad i = 1,2,\dots,NN; \quad j = 1,2\dots,J, \tag{20}$$

where $x^i(j)$ is the jth snapshot of the ith atom motion, J is the number of the snapshots and NN is the number of total degrees of freedom of the molecular model.

There is a choice between computing the singular value decomposition of Q or Q^{T} for finding POM which depends on the relative size of NN and J. In the field of Principal Component Analysis, the first method is called the R-method and second the Q-method [37]. The modal vectors produced by the two methods can be shown to differ by only a constant scaling matrix. In the present paper, the R-method is selected since the number of degrees of the system is not very high. The R-method is described below.

The singular value decomposition of Q is given as

$$[Q] = [U][\Sigma][V]^{\mathrm{T}} \tag{21}$$

where U is a unitary matrix of dimension $NN\times n$ and V is also a unitary matrix of dimension $J\times n$. One may select n and typically n will be much less than J. Note that

$$[U]^{\mathrm{T}}[U] = [I]_{n\times n}, \quad [V]^{\mathrm{T}}[V] = [I]_{n\times n} \tag{22}$$

and Σ is a diagonal matrix of singular values, i.e.

$$[\Sigma]_{n\times n} = \begin{bmatrix} \sigma_1 & & & \\ & \sigma_2 & & \\ & & \ddots & \\ & & & \sigma_n \end{bmatrix}, \tag{23}$$

where

$$\sigma_1 \geqslant \sigma_2 \geqslant \cdots \sigma_n \tag{24}$$

and the correlation matrix Φ is constructed as

$$[\Phi] \equiv [Q][Q]^{\mathrm{T}} = [U][\Sigma]^{\mathrm{T}}[V]^{\mathrm{T}}[V][\Sigma][U]^{\mathrm{T}}. \tag{25}$$

Substituting Eq. (22) into the above equation, we have

$$[\Phi] = [U][\Sigma]^{\mathrm{T}}[\Sigma][U]^{\mathrm{T}} \tag{26}$$

and U is the eigenvector of the matrix $[\Phi]$.

It is well known that the success of the POD methodology depends upon the choice of the excitation used to obtain the snapshots. A certain amount of numerical experimentation may be required to determine an effective excitation to calculate the snapshots.

2.4.1. POM-based reduced order models

The procedure of building POM-based ROM is the same as constructing LNM-based reduced order models except for the transformation matrix between original coordinates, $\hat{x}$, to POD modal coordinates, $\{q\}$.

In this case, the transformation of the coordinates is given as

$$\{\hat{x}\} = [U][\Sigma]\{q\}. \tag{27}$$

Going through the same procedure as before, the governing equations for the reduced order models are given below:

POM-based linear reduced order model without QSC

$$\{\ddot{q}\} + [R]\{\dot{q}\} + [P]\{q\} = k_{\mathrm{s}}B(t)\{W\}, \tag{28}$$

where

$$[R] = ([\Sigma]^{\mathrm{T}}[\Sigma])^{-1}([U][\Sigma])^{\mathrm{T}}[M]^{-1}[C][U][\Sigma] = 2\xi\omega_1[I],$$
$$[P] = ([\Sigma]^{\mathrm{T}}[\Sigma])^{-1}([U][\Sigma])^{\mathrm{T}}[M]^{-1}[K]([U][\Sigma]),$$
$$\{W\} = ([\Sigma]^{\mathrm{T}}[\Sigma])^{-1}([U][\Sigma])^{\mathrm{T}}[M]^{-1}\{\delta(i-k)\}.$$

POM-based nonlinear reduced order model without QSC

$$\{\ddot{q}\} + [R]\{\dot{q}\} - [\pi]\{F_{\mathrm{N}}\} + [\pi]\{F_{\mathrm{e}}\} = k_{\mathrm{s}}B_t W, \tag{29}$$

where $[R]$ and $[W]$ are same as in Eq. (28) and

$$[\pi] = ([\Sigma]^{\mathrm{T}}[\Sigma])^{-1}([U][\Sigma])^{\mathrm{T}}[M]^{-1}.$$

2.5. Reduced order modeling using component modal synthesis (CMS)

Reduced order model can also be constructed by means of component modal synthesis using the POM for each component. Assume that the structure in Fig. 1 is composed of m substructures, $r = 1, 2, \ldots, m$. For substructure r, the displacement vector, $\{x\}_r$, can be represented by a matrix with POM as columns multiplied by a N_r-dimensional time-dependent modal coordinate vector, $\{q\}_r$,

$$\{x\}_r = \{x_{\mathrm{s}}\}_r + \{\hat{x}\}_r = \{x_{\mathrm{s}}\}_r + ([U][\Sigma])_r\{q\}_r. \tag{30}$$

Define vectors

$$\{x\}_d = \{\{x\}_1^{\mathrm{T}}, \{x\}_2^{\mathrm{T}}, \ldots, \{x\}_m^{\mathrm{T}}\}^{\mathrm{T}},$$
$$\{q\}_d = \{\{q\}_1^{\mathrm{T}}, \{q\}_2^{\mathrm{T}}, \ldots, \{q\}_m^{\mathrm{T}}\}^{\mathrm{T}}$$

and matrices

$$[T] = \mathrm{diag}(([U][\Sigma])_r), \quad r = 1, 2 \ldots, m,$$
$$[M]_d = [T]^{\mathrm{T}}\mathrm{diag}([M]_r)[T], \quad r = 1, 2 \ldots, m,$$

where $\{q\}_d$ is the N-dimensional disjoint POD modal coordinator vector with $N = \sum_{r=1}^{m} N_r$.

Assuming the substructures act independently of each other, the combined kinetic energy of the assembled structure is

$$T = \sum_{r=1}^{m} T_r = \sum_{r=1}^{m} \frac{1}{2} \{\dot{x}\}_r^{\mathrm{T}} [M]_r \{\dot{x}\}_r = \frac{1}{2} \{\dot{q}\}_d^{\mathrm{T}} [M]_d \{\dot{q}\}_d. \tag{31}$$

Similarly, the combined potential energy function is

$$V = \sum_{r=1}^{m} V_r, \tag{32}$$

where V_r is a function of $\{q\}_r$.

However, in the assembled structure each substructure is subjected to forces exerted by other substructures. Thus the total potential energy is modified to

$$V = \sum_{r=1}^{m} V_r + V_{\text{inter}}, \tag{33}$$

where V_{inter} is the interaction energy between substructures and is a function of $\{q\}_d$. Thus, the atoms at the interface of each two substructures must satisfy some geometric compatibility conditions. For the structure in Fig. 1, considering two neighboring substructures r and t, one must have

$$x_{j,r} = x_{j,t}, \tag{34}$$

where j's are the degrees of freedom associated with the atoms at the interface between the adjoint substructures. Suppose there are N_j such constraints to connect substructures. Then the entire system has only $n = N - N_j$ degrees of freedom. Let $\{q\}$ be the n-dimensional vector of POM coordinates, $\{q\}$ is related to $\{q\}_d$ as

$$\{q\}_d = [C]\{q\}, \tag{35}$$

where $[C]$ is an $N \times n$ rectangular constraint matrix.

Insert Eq. (35) into Eqs. (31) and (33), and then the governing equations of motion in terms of $\{q\}$ can be obtained by Lagrange Equations. For a detailed description of component modal synthesis, see [38].

3. Results

In this section, simulations are made to demonstrate the accuracy of the modal reduction methods described in Section 2. A simple biological system, one monomer of α-D-glucopyranose, is considered first in Section 3.1–3.3. In this system, there are 24 atoms with 6 carbon atoms, 6 oxygen atoms and 12 hydrogen atoms. Two of these atoms are fixed and one is attached to the tip of the AFM and only allowed to move in one direction as shown in Fig. 1. Therefore, the number of degree of freedom is $n = 21 \times 3 + 1 = 64$. In Section 3.4, a ten monomer amylose is considered. The stiffness of the AFM cantilever is chosen to be $k_s = 10$ pN/Å. The force field parameters are obtained from Ref. [34]. In the simultions, the AFM base motion is prescribed along z-direction as

$$B(t) = A \sin(2\pi f t),$$

where A and f are the excitation amplitude and frequency, respectively.

3.1. Results from linear ROM

The static equilibrium state is the "chair-like" state shown in Fig. 2 obtained using the original nonlinear equations. The eigenvalues and eigenvectors for this conformation are computed using the perturbation

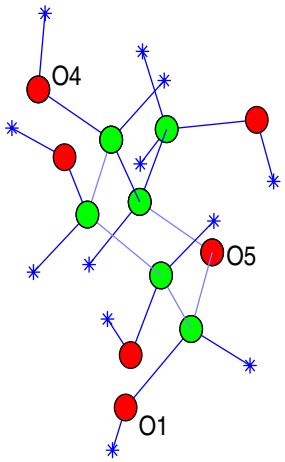

Fig. 2. Chair-like state of a single α-D-glucopyranose monomer. The symbol ✻ denotes Hydrogen atoms and the symbol ● is for carbon or oxygen atoms.

equation, Eq. (7), when the external excitation is removed and the damping is set to zero. The first 20 eigenvalues are shown in Table 1. All the eigenvalues are shown in Fig. 3.

It is obvious from Fig. 3 that there are jumps in the distribution of eigenvalues or natural frequencies. This is probably because the monomer includes 12 hydrogen atoms which are significantly lighter than

Table 1
Eigenvalues, f_i (THz)

$f_{1–5}$	$f_{6–10}$	$f_{11–15}$	$f_{16–20}$
1.46346e − 001	3.94122e + 000	1.02265e + 001	1.37841e + 001
1.04667e + 000	4.55072e + 000	1.14259e + 001	1.45702e + 001
1.77876e + 000	5.48644e + 000	1.23014e + 001	1.57309e + 001
2.91688e + 000	5.83528e + 000	1.24758e + 001	1.65451e + 001
3.04658e + 000	8.79735e + 000	1.29923e + 001	1.69857e + 001

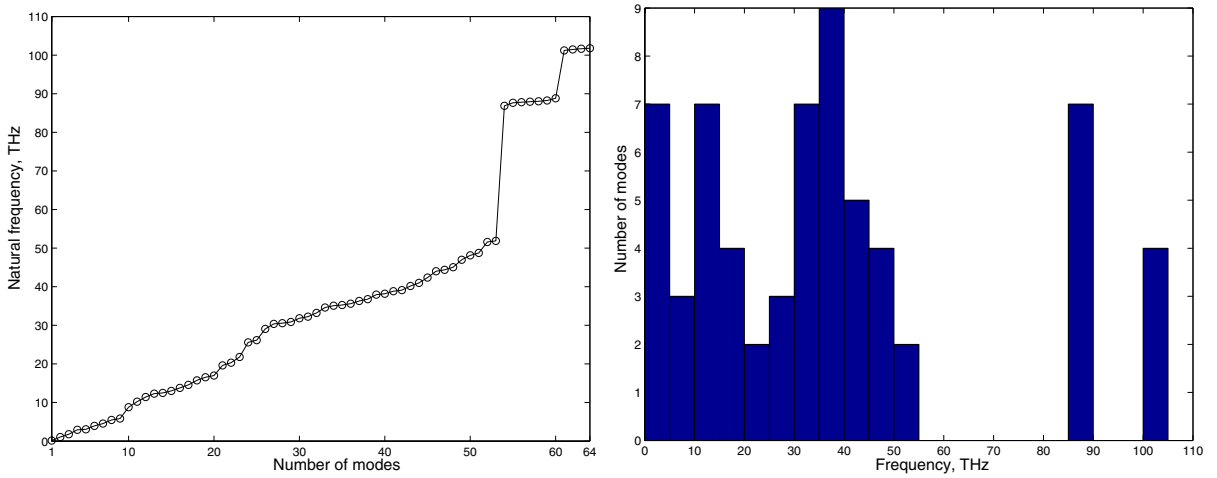

Fig. 3. Natural frequencies.

other atoms and the strength of the various bonds is quite different. Such jumps are common in molecular spectra and the similar cases are also seen in other literature such as [39–41]. In [41], the authors stated that the different frequency modes are associated with different bond stretching, angle bending and librations of side chain groups.

Define the RMS magnitude of each atom as

$$s_i = \sqrt{(x^i_{,\mathrm{rms}})^2 + (y^i_{,\mathrm{rms}})^2 + (z^i_{,\mathrm{rms}})^2}. \tag{36}$$

Also in order to compare the results obtained from the ROM and the solution calculated by appplying a time marching method to the original system described by Eq. (5), the total RMS error, err, is defined as

$$\mathrm{err} = 100\sqrt{\frac{1}{N}\sum_{i=1}^{N}\frac{(s_{i,\mathrm{Full}} - s_{i,\mathrm{ROM}})^2}{s^2_{i,\mathrm{Full}}}}\%, \tag{37}$$

where N is the total number of atoms in motion.

Fig. 4 shows the total rms error compared to the exact solution vs. the number of modes included in the linear ROM with and without the QSC (Eqs. (9) and (13)) for $A = 1$ Å. The excitation frequency is $f = 100$ GHz which is below the first natural frequency shown in Table 1. As expected, the total error decreases as the number of modes included in the linear ROM with or without the QSC increases. When the number of modes included in the ROM is low, the result obtained from the linear model with the QSC is generally much better than the result using the linear model without the QSC. For example, when using the model without the QSC the total rms error is 21.2% while the total rms error is 0.1% with the QSC if only one mode is included in both models. When the number of modes retained in ROM increases, the results from the two linear models get closer and closer. Finally when the number of modes included in the ROM is large enough, the difference between the results from both models is negligible. Therefore, QSC is important in the simulation using reduced order models especially in the case with only a few modes included. Thus, the dimension of the system can be further reduced with QSC.

Fig. 5 shows the total rms error vs. the number of modes included for different excitation amplitudes, $A = 10$ Å and $A = 30$ Å, with the frequency of $f = 100$ GHz. The results in Fig. 5 have a similar trend as for the case with $A = 1$ Å in Fig. 4.

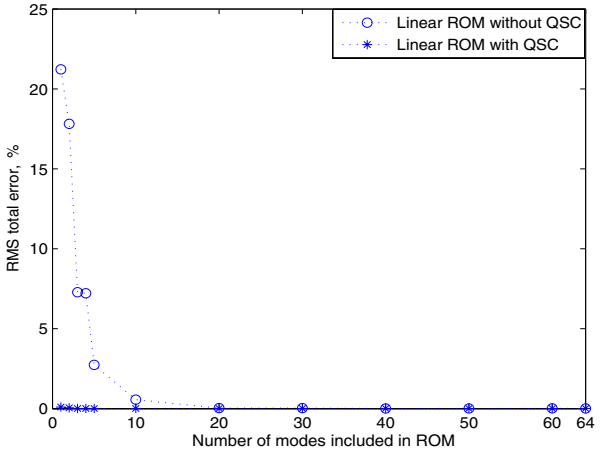

Fig. 4. Total RMS error vs. number of eigenmodes for $A = 1$ Å and $f = 100$ GHz, using the linear ROM without and with QSC.

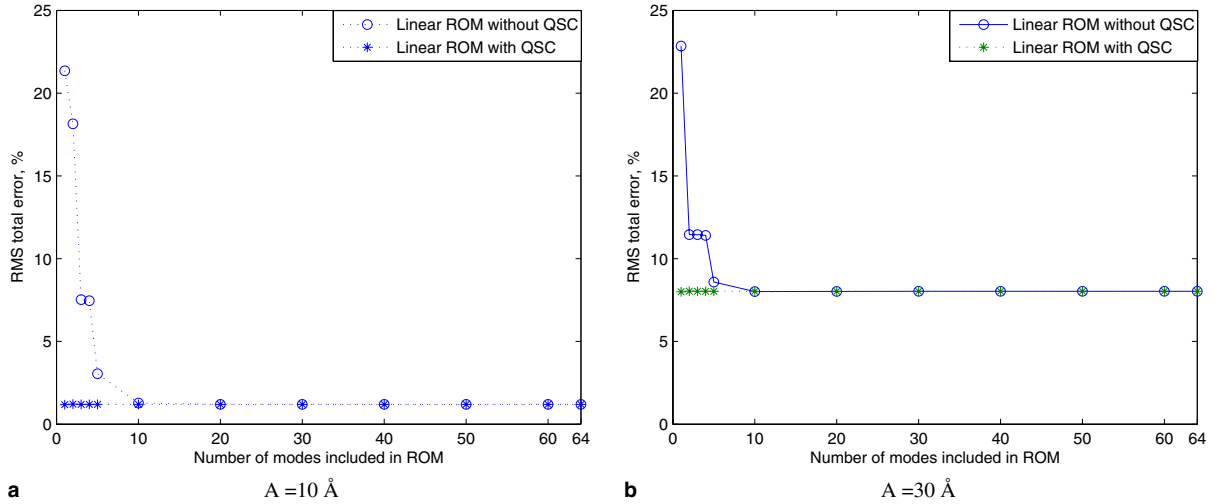

Fig. 5. Total RMS error vs. number of eigenmodes for different excitation amplitudes with $f = 100$ GHz, using the linear ROM with and without QSC.

To see to what extent the linear ROM can accurately represent the response of the system, different frequency and different amplitude excitations are considered. The total rms error vs. the excitation amplitude using fully linear models as described by Eq. (7) for an excitation frequency of 100 GHz is shown in Fig. 6. As the excitation amplitude increases the total error increases when the excitation amplitude is lower than $A = 50$ Å. Surprisingly the error begins to decrease beyond that. Actually when the excitation amplitude is 40 Å, the responses of atoms already have higher order harmonic components. For illustration, the time histories of atom O5 in x-direction for different excitation amplitude are shown in Fig. 7. For comparison the linear results for the excitation frequency of 2 THz are also shown in Fig. 6. It is obvious that at the higher excitation frequency, the linear results are worse given the same excitation amplitude. Thus the results in Fig. 6 suggest that linear perturbation is only valid for small amplitude and low frequency excitations.

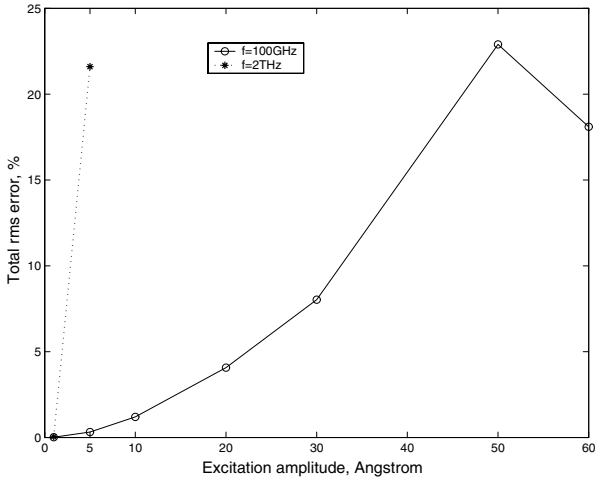

Fig. 6. Total RMS error vs. the excitation amplitude using the linear perturbation model.

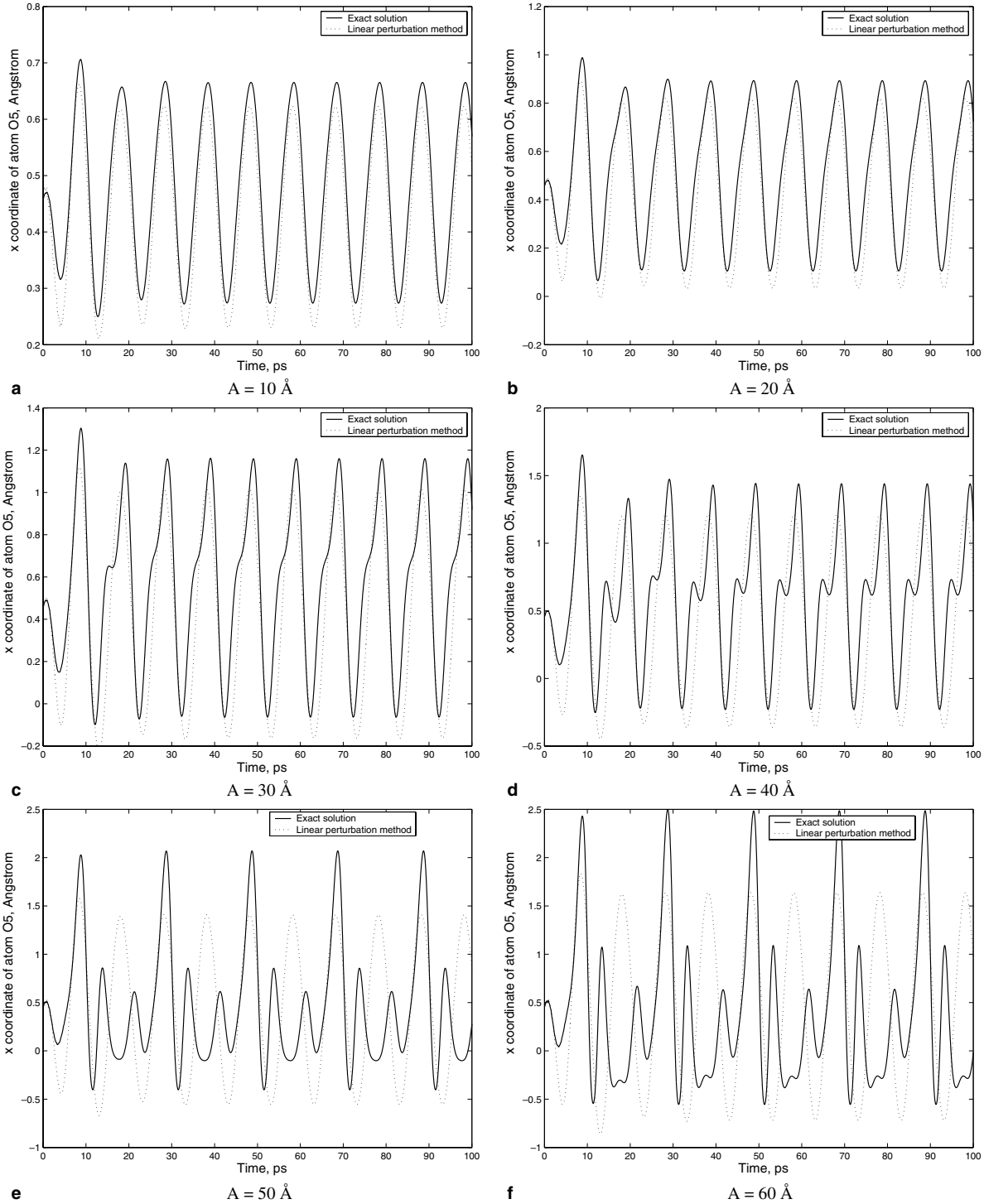

Fig. 7. Time histories of x-direction displacement of atom O5 for different excitation amplitudes and excitation frequency of $f = 100$ GHz.

3.2. Results from nonlinear ROM without QSC

In this section, a nonlinear reduced order model without QSC is investigated. Two sets of basis vectors are used in the simulations. One is the eigenspace composed of linear normal modes (LNM) and the other is the space spanned by POM. The LNM-based and POM-based nonlinear ROMs are described by Eqs. (14) and (29), respectively. The computation of linear normal modes is straightforward. Assume the shape of potential energy in the neighborhood of the equilibrium state is characterized by the Hessian matrix (stiffness matrix) with respect to the Cartesian coordinates and then solve the standard eigenvalue problem. The procedure for calculating POM is described in Section 2.4.

In this section, the snapshots are generated by first exciting the system by a sine-sweep with lower and upper limit frequencies of ω_{low} and ω_{up} given as

$$B(t) = A_{\text{sweep}} \sin\left(\omega_{\text{low}} + \frac{(\omega_{\text{up}} - \omega_{\text{low}})t}{2T}\right)t,$$

where T is the sweep period.

The data from the time history of the response is used to create the correlation matrix, Q. After Q is generated, the POM are calculated as described in Section 2.4. The POM used in the simulations are obtained from time simulations of Eq. (5) if not otherwise specified.

First, consider the case in which the excitation amplitude and frequency are $A = 1$ Å and $f = 100$ GHz, respectively. In this case, we choose f_{low}=0, and f_{up}=2 (THz) and $T = 20$ ps.

The eigenvalues of the POD correlation matrix are shown in Fig. 8.

Fig. 9 shows the rms amplitude of each atom for different number of LNM or POM retained. For the ROM based on LNM, the results obviously get closer to the exact solution when the number of modes included increases from 1 to 5. But the results only show a slight difference when more than five modes are included. Compared to the ROM based on LNM, POD yields a significantly better approximation. The results from POD approach the exact solution quickly as the number of modes included increases. The total rms error is 21.2% when 5 POM are included and is only 0.01% when 10 POM are included.

Fig. 10 shows the total rms error vs. the number of LNM or POM in the ROM. It is found the results from the ROM based on LNM converge to the exact solution much more slowly than the results obtained from the ROM with POM as the basis. For the LNM the results agree well with the exact solution when full

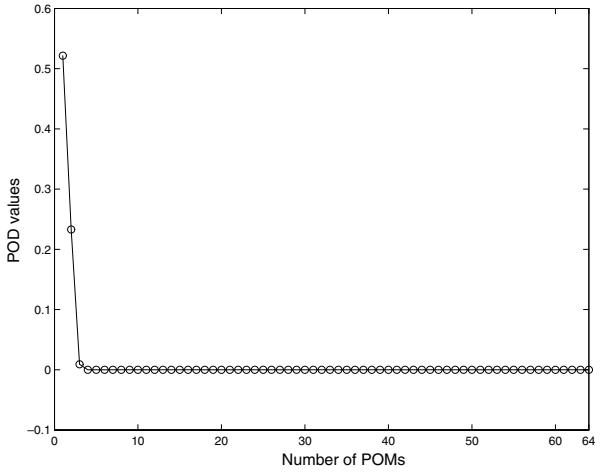

Fig. 8. POD values vs. number of POD modes.

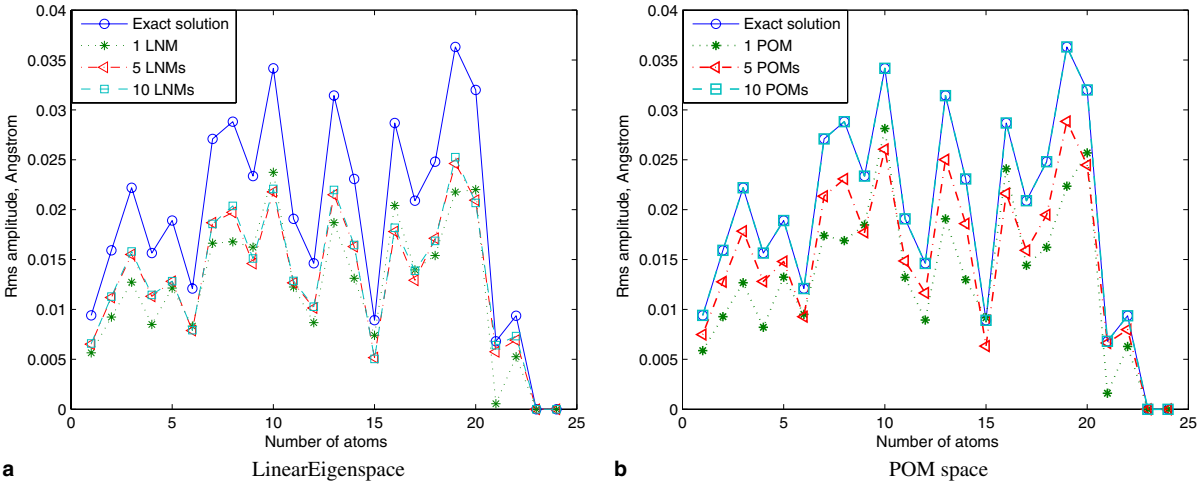

Fig. 9. Rms amplitude of each atom for different number of modes included in ROM. $A = 1$ Å and $f = 100$ GHz.

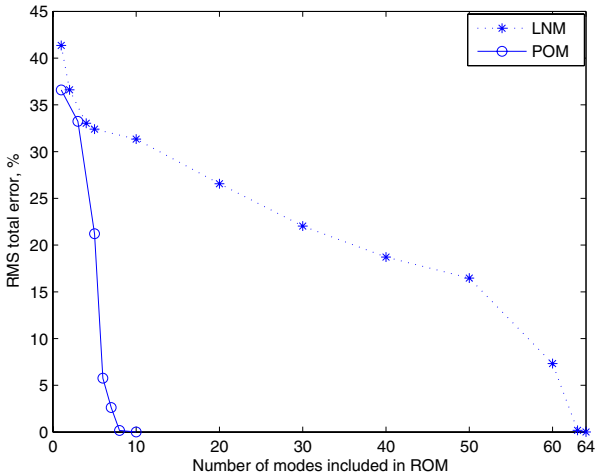

Fig. 10. Total rms error vs. number of LNM or POM included in ROM. $A = 1$ Å and $f = 100$ GHz.

model is used and the error goes up significantly even though only few high frequency modes are truncated in the ROM. This is probably because linear eigenmodes are no longer invariant manifolds. Reduced order models based on LNM cannot capture the essential dynamics by simply truncating the high frequency modes similar to the case discussed in [9].

When the excitation amplitude increases, the trend of the results from the ROM based on LNM or POM appear similar to those for the case in which the excitation amplitude is 1 Å. For illustration, the total rms vs. number of modes included in ROM for different excitation amplitudes is shown in Fig. 11. For large amplitude excitation, the results obtained by the ROM with LNM as basis vectors converge extremely slowly and the results are unacceptable even when only few modes are removed. On the contrary, POD gives good results.

In summary, the nonlinear ROM based on LNM fails to give good results and the ROM based on POM works much better for complex nonlinear systems and shows advantages over linear models.

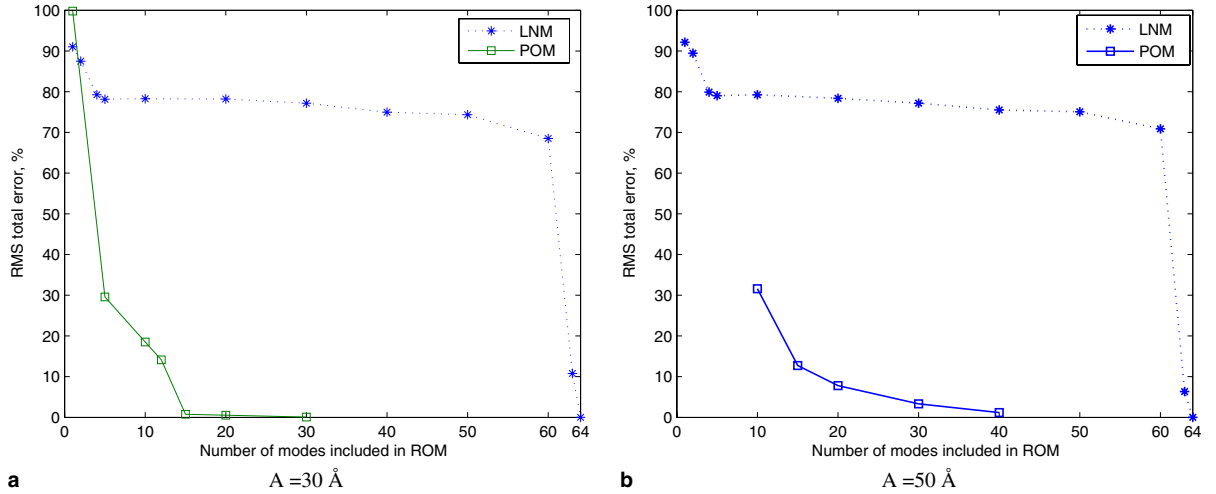

Fig. 11. Total rms error vs. number of LNM or POM included in ROM for different excitation amplitudes. $f = 100$ GHz.

3.2.1. Discussion of the ROM with the basis of LNM

To understand why the ROM based on the LNM fails, Fig. 12 shows how the temporal mean of x_i drifts when using the ROM for $A = 1$ Å and $A = 30$ Å, respectively. Note however that the rms amplitudes of the modal coordinates obtained from the full model shown in Fig. 13 do suggest that only a few low frequency modes make an essential contribution to the response. Here the harmonic excitation frequency is 100 GHz. The deviation is compared to the temporal mean for the exact solution. The deviation of the ROM mean is defined as

$$d = \sqrt{\sum_{i=1}^{n} (\langle x_i \rangle_{\mathrm{ROM}} - \langle x_i \rangle_{\mathrm{exact}})^2 / n},$$

where $\langle \cdot \rangle$ denotes temporal mean and n is the number of DOF of the system.

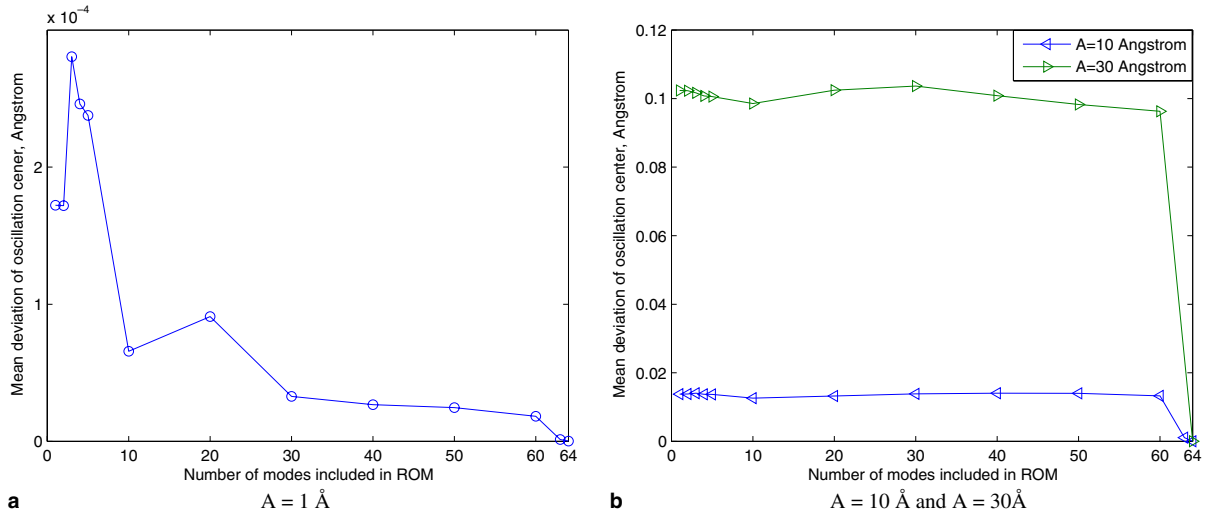

Fig. 12. Mean deviation of oscillation center vs. number of LNM included in ROM for different excitation amplitudes. $f = 100$ GHz.

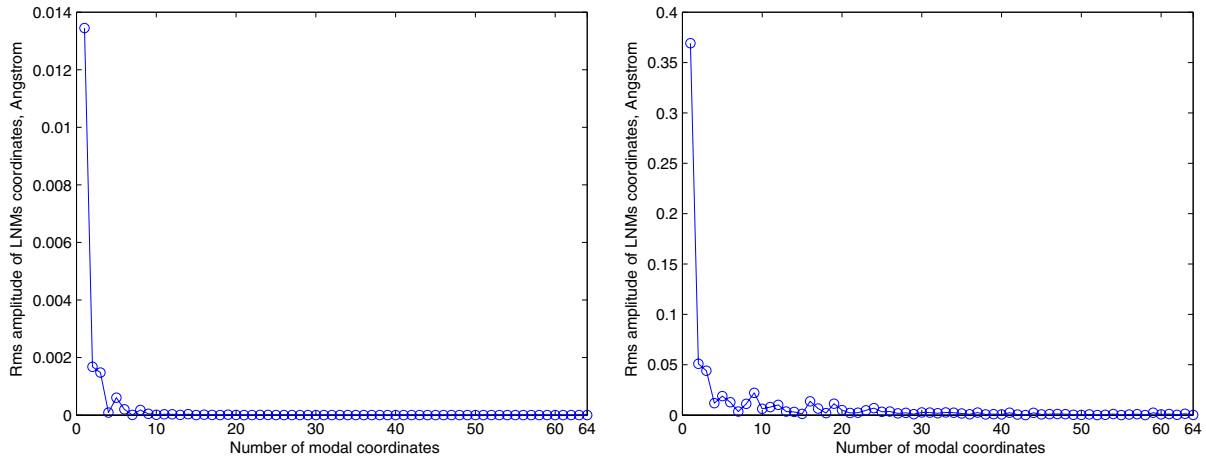

Fig. 13. Rms amplitude of LNM coordinates vs. number of modes. $f = 100$ GHz.

The results in Fig. 12 clearly indicate that the ROM temporal mean shifts away from the exact temporal mean as the number of modes decreases. When the excitation amplitude gets larger this shift is very dramatic (see Figs. 12(b) and 11(a)). This is probably due to the strong coupling between higher and lower modes. Fig. 14 shows the phase portraits of some modal coordinates for the fully nonlinear model. The initial equilibrium state corresponds to $q_i = 0$ for all i. It is noted that the oscillations occur about the original static static state (conformation) for the lower modes, but the temporal mean of the oscillation shifts substantially for the higher modes. Initially the system stays in one equilibrium state. However, once the oscillation starts, the energy minima of the high-frequency modal coordinates are shifted because multiple equilibrium states exist in a small region and the system reaches the well of the new equilibrium under the action of external force.

In addition to the shifting of the oscillation center, another important factor is the stiffening due to modal truncation. Fig. 15 shows the rms amplitude of modal coordinates obtained by the ROM with different number of modes included. It is clearly shown that the rms amplitude of the first modal coordinate significantly decrease as the number of modes removed increases. For large amplitude excitation this effect is more pronounced. The rms amplitudes of the first few coordinates in the ROM are smaller than the corresponding results in the full model.

In summary, the shifting of the oscillation center and the stiffening of the system provide an explanation of why the ROM based on LNM gives a poor approximation of the response. This is similar to the case discussed in [26].

3.2.2. Sensitivity study of POM

Recall that POM are data dependent. Fig. 16 shows the total rms error vs. number of modes included in the ROM for different basis vectors. The results denoted by the dotted line with circles are obtained from the ROM with the basis vectors of the POM calculated from time simulation of linear, small perturbation equations (Eq. (7)). As expected the trend is similar to the ROM based on LNM since the correlation matrix reflects the same characteristics of the linear systems. Therefore, the POM obtained from the linear perturbation model are not good for nonlinear reduced order models.

Also the results from the ROM based on the POM obtained from the snapshots of the response corresponding to sine-sweeps with different upper limit frequencies are shown in Fig. 16. These suggest that the appropriate choice for the frequency range of the sine sweep can make the ROM more efficient. In this case, the

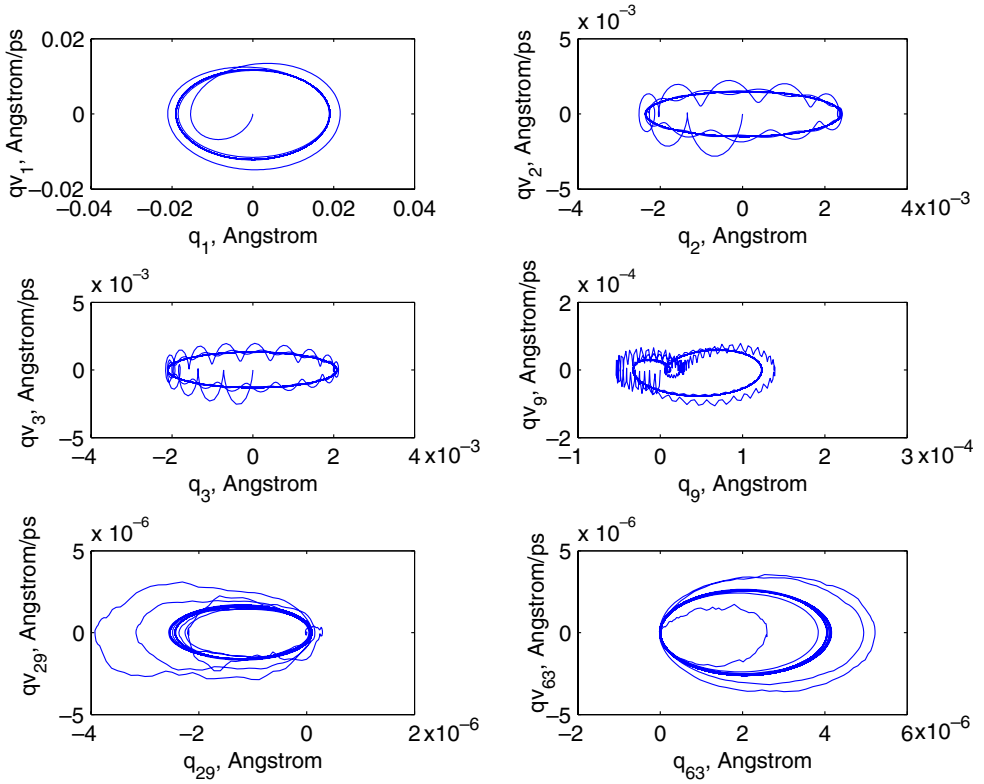

Fig. 14. Phase plots in LNM space. $A = 1$ Å and $f = 100$ GHz. qv denotes the corresponding modal speed.

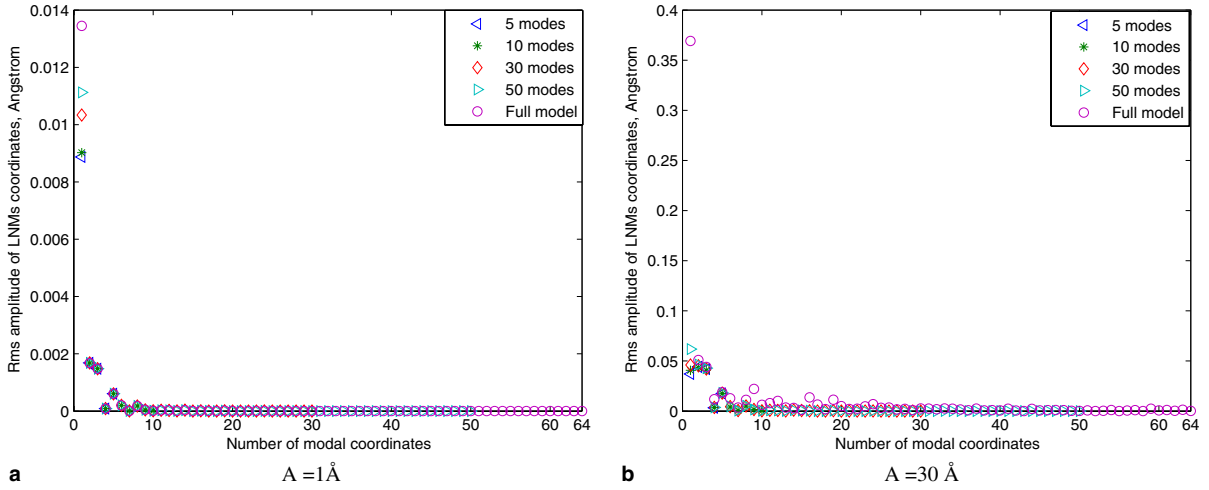

Fig. 15. Rms amplitude of LNM modal coordinates vs number of modes obtained by the ROM with different number of modes included for $A = 1$ Å and $A = 30$ Å. $f = 100$ GHz.

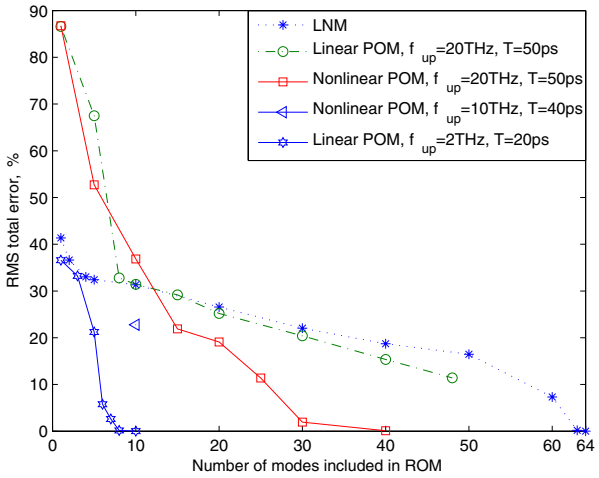

Fig. 16. Total rms error vs. number of LNM or POM included in ROM. $A = 1$ Å and $f = 100$ GHz.

harmonic excitation frequency is 100 GHz which is below the first natural frequency and a decrease of the upper limit frequency of the sine sweep can reduce the number of modes necessary in the ROM to satisfy a given level of accuracy. Thus a prior knowledge of the system dynamics does help to choose a good set of POM.

The POM used in the previous simulations are generated from the time simulations excited by the sine sweep with the same amplitude as the harmonic excitation. There is a question arising about this. Can the POM obtained in one case for one choice of excitation amplitude work for other cases? To answer this, several sets of POM are created from different amplitude sine-sweeps. Figs. 17(a) and (b) and 18 show the total rms error vs. number of POM included in ROM with the basis vectors determined from different amplitude sine-sweep excitations for $A = 1$ Å, $A = 30$ Å and $A = 50$ Å, respectively. The harmonic excitation frequency is again chosen to be 100 GHz. For comparison, the results obtained by the ROM based on LNM are also plotted. Although the results from different POM vary slightly, the agreement is good compared to the results based on LNM even for large amplitude excitation. Fig. 17(c) and (d) shows the total rms error vs. number of POM included in ROM with the basis vectors determined from different amplitude sine-sweep excitations for $f = 2$ THz and $A = 1$ Å, $A = 5$ Å, respectively. Again, it shows POM obtained in one case can be used in the other case.

Therefore, the POM obtained from one case are valid for a wide range of other cases.

3.3. Results from nonlinear ROM with QSC

In Section 3.1, it is noted that the QSC can improve the linear ROM and make the model more efficient. In this section, the effects of the QSC on the nonlinear ROM are also studied. The nonlinear reduced order model with the QSC is described by Eq. (19). All the ROMs used in this section are LNM-based.

Fig. 19 shows the total rms error vs. number of LNM included in the ROMs described by Eqs. (9), (13), (14) and (19) for different amplitude and different frequency excitations. For nonlinear ROMs, the benefit of the QSC is not as obvious although it gives a slightly better results in Fig. 19(a) and (c). For high-frequency excitation, the effect of the QSC is undetectable even when few modes are included in the ROM (see Fig. 19(b) and (d)).

In Fig. 19(a), the square symbol denotes the results obtained from the ROM based on LNM when using Taylor series to approximate the potential forces. One purpose of this calculation is to check why there is such a large difference when the same number of modes are included in the ROM and also why the linear

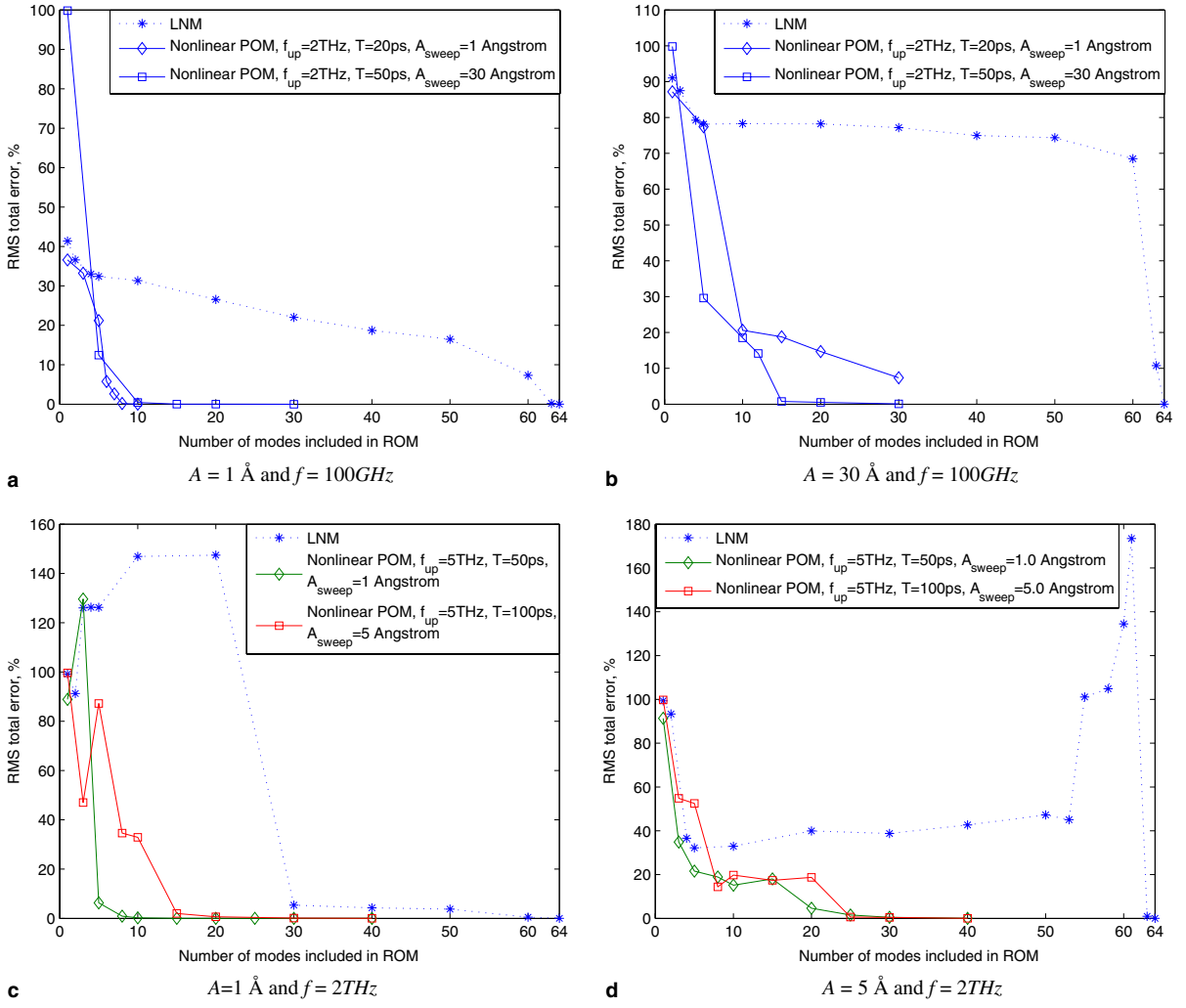

Fig. 17. Total rms error vs. number of LNM or POM included in ROM for different cases.

results seem much better than the corresponding nonlinear results. Fig. 19(a) shows that the results approximate the linear results when the forces are expanded up to the order of three and the results agree well with nonlinear ROM when higher order terms are included. This implies that the strong nonlinearity makes the system quite sensitive.

3.4. Results from nonlinear ROM using POD and CMS

To demonstrate the validity of component modal synthesis described in Section 2.5, a ten-monomer amylose chain is considered. In this case, the two adjoint substructures are connected through O1–O4 linkage. Thus there are three constraints for connecting each of the two neighboring substructures. The POM for each substructure are calculated from an ensemble of data obtained by running the full model simulation. Then the reduced order model is constructed by the procedure described in Section 2.5. In this section, the harmonic excitation is chosen to have an amplitude of 1 Å and a frequency of 20 GHz.

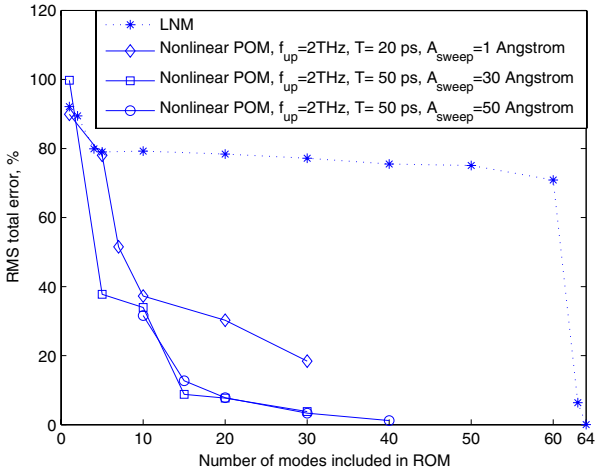

Fig. 18. Total rms error vs. number of LNM or POM included in ROM. $A = 50$ Å and $f = 100$ GHz.

Fig. 20 shows the total rms error vs. number of POM included in each substructure for ten substructures. As expected the error decreases as the number of POM per substructure included in ROM increases.

The total rms error vs. number of substructures for various numbers of total degrees for the assembled structure is shown in Fig. 21. Note that in the figure N is the total number of degrees of the system before the component mode synthesis. It is clear that the error increases as the number of substructures increases. This is explained in part by the fact that the error comes from the geometric compatibility conditions. When two substructures are joined together, half of the joint degrees of freedom are removed. With a decrease in the number of substructures, the number of joint degrees of freedom that are removed is smaller compared to the number of degrees of freedom in the substructure and thus the results become more accurate. Hence, given a desired accuracy, fewer substructures are expected to give more accurate results if the total number of degrees of freedom is fixed.

To reduce the model further, one can carry out another POD procedure as described in Section 2.4 after the ROM using POD and CMS is obtained. For example, Fig. 22 shows the results for the case in which 10 substructures are considered and each substructure includes 30 modes. The symbol * denotes the results obtained from the POD for the original system. The results obtained by CMS and POD agree well with the results from the POD for the entire structure.

3.5. Efficiency of reduced order models

The computational cost is proportional to the number of calculations carried out in the simulations. And the number of calculations in one simulation is

$$N_c = N_{c1} N_t,$$

where N_{c1} is the number of calculations each time step and N_t is total number of time steps.

To make the computation more efficient one needs to reduce N_c. More specifically, one needs to decrease N_{c1} or N_t or both. The efficiency of the reduced order models presented in this paper is discussed next.

3.5.1. Linear reduced order models

Comparing Eq. (5) with Eq. (7), when the nonlinear system of equations are linearized, the complex potential force term in Eq. (5) (see Appendix A in [32]) is simply reduced to a matrix–vector multiplication.

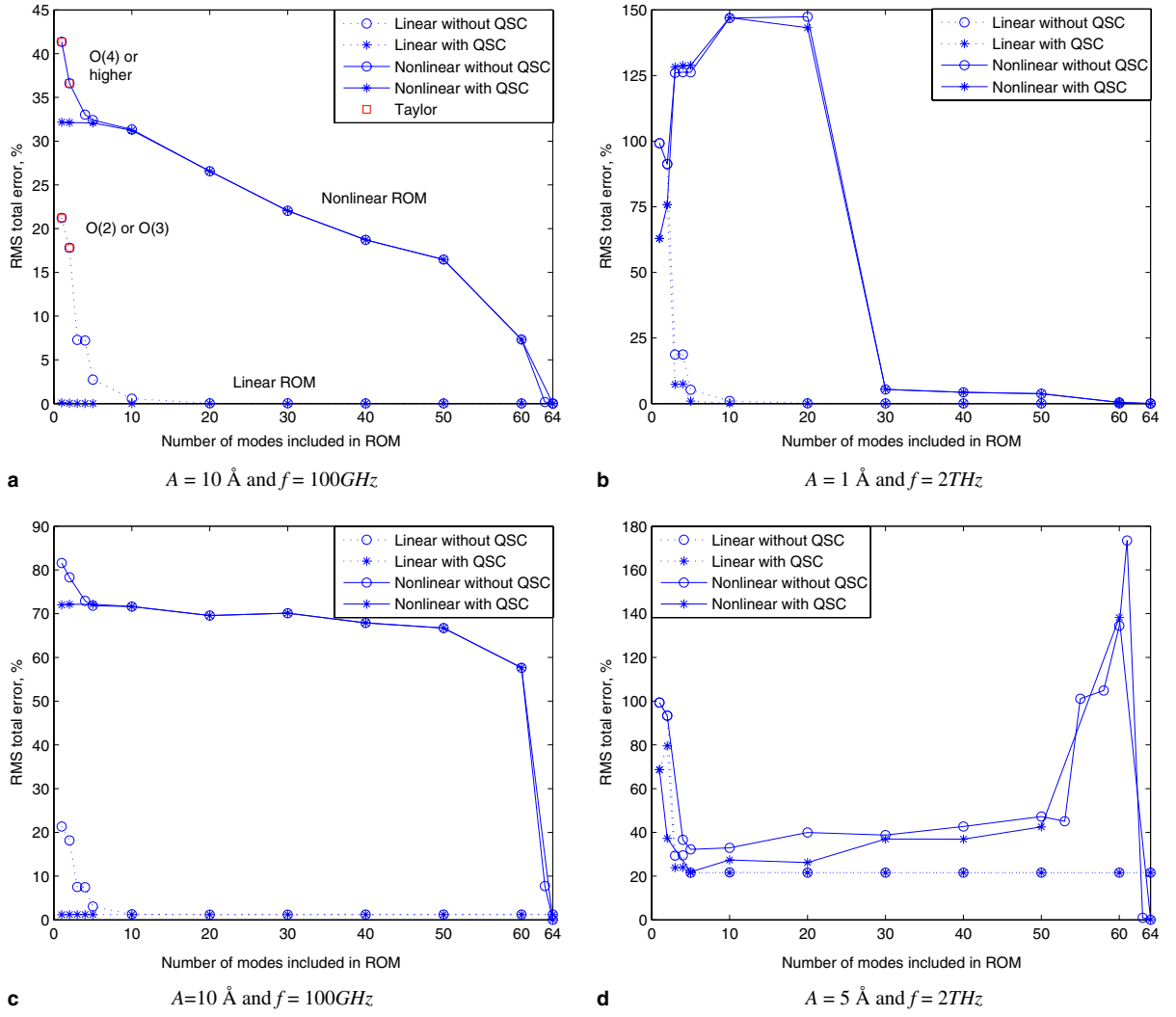

Fig. 19. Total rms error vs. number of LNM included in ROM for different cases.

The Hessian matrix is calculated once for all and the computation of matrix–vector is the order of n, where n is the dimension of the matrix in Eq. (7). Thus N_{c1} can be reduced by a factor of 5–10. This number is obtained by running the program for one monomer under the same condition since the potential forces are so complicated that it is difficult to count the number of calculations. Also N_{c1} can be further reduced by using modal reduction. Furthermore, the computation can be made more efficient by reducing N_t. Recall that the integration time step is inversely proportional to highest frequency of the system. The time step can be made larger since the high frequency modes in the system are truncated in the reduced order models. Especially for low frequency excitations only a few modes are required and the computation cost can be reduced by a factor of ten or even one hundred since the highest frequency is much larger than the lowest frequency. In our case for one monomer the highest natural frequency is almost a thousand times the lowest frequency.

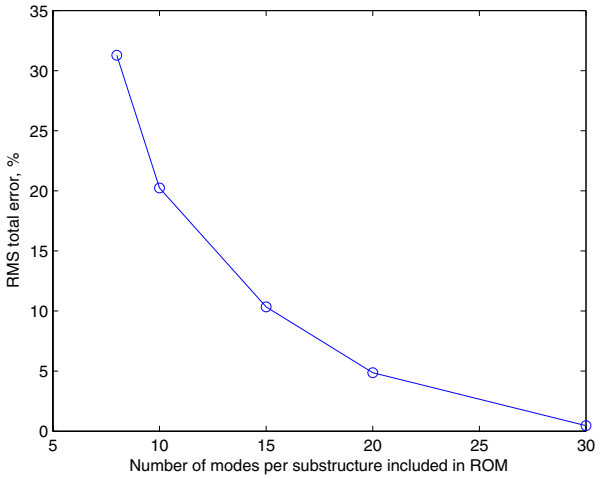

Fig. 20. Total rms error vs. number of POM per substructure included in ROM. $A = 1$ Å and $f = 20$ GHz.

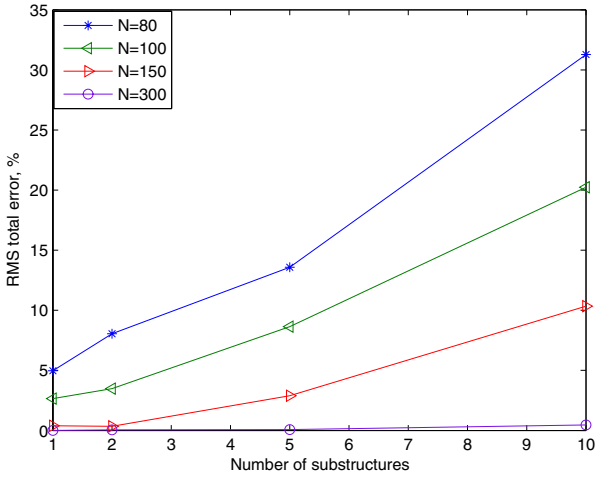

Fig. 21. Total rms error vs. number of substructures included in ROM. $A = 1$ Å and $f = 20$ GHz.

3.5.2. Nonlinear reduced order models

Compared to linear reduced order models, the efficiency of nonlinear reduced order model is more modest since the complex potential forces need to be evaluated in both the original system and the reduced order models. The computational cost using nonlinear reduced order models based on LNM (Eq. (14) and Eq. (19)) for one monomer *using the same time step* is shown in Fig. 23 for the case with the excitation of $A = 1$ Å and $f = 100$ GHz. In Fig. 23, it is observed that the computational time for the ROM is usually larger than the time required by the original system when *using the same time step* (Note that in the figure the relative time is defined to be the ratio of the computational time for the ROM to that of the original system). This is because in the ROM additional time is needed for the matrix–vector multiplication. However, the computation for the ROM can be reduced by increasing the integration time step as in the linear case. A dramatic decrease of the number of time steps, N_t, can be expected to speed up the calculation for

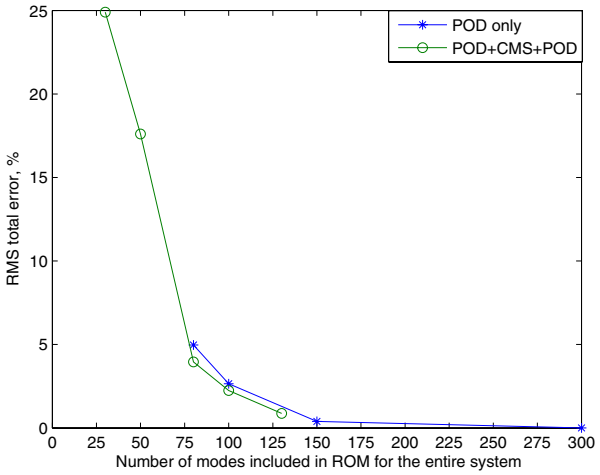

Fig. 22. Total rms error vs. number of modes in ROM for the entire system. $A = 1$ Å and $f = 20$ GHz.

low frequency excitation. It should also be mentioned however, that the time step cannot always be reduced as much as for the linear case since high harmonic components may exist in the nonlinear response. But for the amplitude considered here, the time step can still be reduced by a factor of up to a hundred which means the calculation can be up to one hundred times faster depending on the number of modes included in the ROM. The additional time and cost for matrix calculation is negligible.

3.5.3. Nonlinear reduced order models using POD and CMS

Comparing Eq. (30) with Eq. (27), it is found that the original physical coordinates have a similar relationship with the corresponding generalized coordinates except for the transformation matrices. Thus the governing equations of motion are similar. Therefore, the efficiency of the nonlinear reduced order models is comparable to that of the nonlinear model using LNM. As an example, Fig. 24 shows the

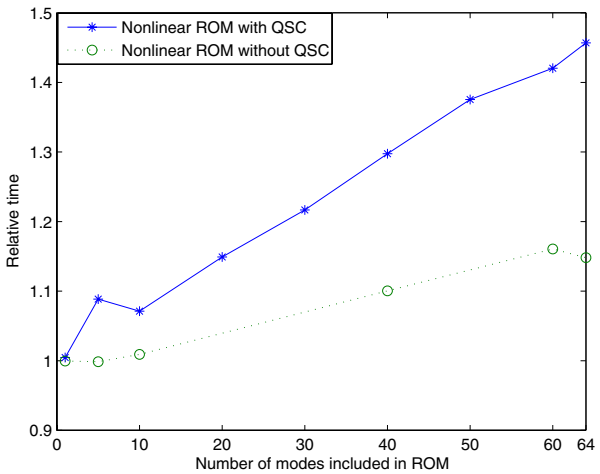

Fig. 23. Computational cost for the excitation of $A = 1$ Å and $f = 100$ GHz compared to the fully nonlinear simulation using the same time step.

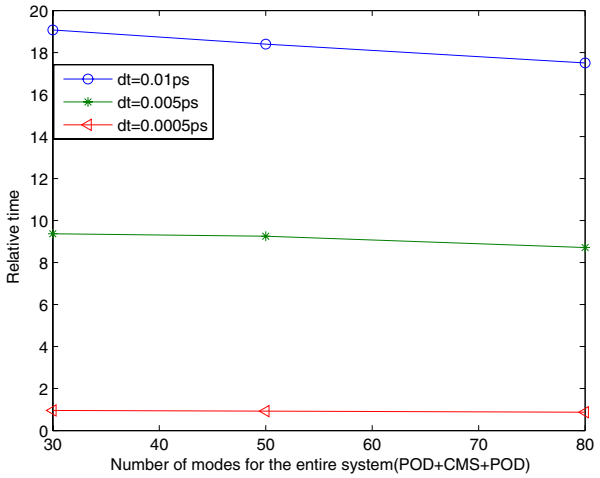

Fig. 24. Relative time vs. number of modes for the entire system for different time steps. $A = 1$ Å and $f = 20$ GHz.

relative time vs. the number of modes used in the entire system. In this case, POD is carried out after the CMS model is built. In the plot the relative time is defined to be the ratio of the computational time for the original system to that of the ROM. Thus larger relative times are desirable. It is clear the time and cost can be significantly reduced by a factor of up to 20 by increasing the time step without changing the accuracy. Also it is noted that as the time step gets larger, the models of lower dimension also have a higher relative time.

4. Conclusions

A detailed study of modal reduction based on LNM and POM has been carried out in modeling a α-D-glucopyranose monomer and also a chain of monomers under harmonic AFM base excitation. It has been demonstrated that the linear reduced order model (ROM) is valid for small amplitude excitation and low frequency excitation. The nonlinear reduced order model with LNM as the basis vectors is less useful in modeling the molecules with a strong nonlinearity. Fortunately, the nonlinear reduced order model based on POM provides a good approximation even for large amplitude or high frequency excitation. It is shown that the quasi-static correction plays an important role when only few modes are included for the linear ROMs but has little effect in the nonlinear case. Also it is important to note that the POM obtained in one case for a given amplitude of excitation is applicable for a wide range of cases.

The reduced order model based on component modal synthesis using POM for each component is also constructed. Although the POM for each component are calculated from the full model simulation, CMS makes the eigenvalue problem of the correlation matrix more tractable and more efficient. Since there are many complicated and large biological molecules in the nature, the combination of CMS and POD may provide a useful method for modeling their dynamic behavior.

With the reduced order system, the computational time and cost can be significantly reduced by a factor of ten or even a hundred depending on the external excitations and whether the linear or nonlinear model is used in the simulation.

Therefore, modal reduction is a possible, effective way to decrease the computational time and cost of a molecular dynamics simulation.

References

[1] P.P. Ewald, Die Berechnung optischer und elektrostatischer Gitterpotentilae, Annals of Physics 64 (1921) 253–287.
[2] J.W. Eastwood, R.W. Hockney, Shaping the force law in two-dimensional particle mesh models, Journal of Computational Physics 16 (1974) 342–359.
[3] L. Greengard, V. Rokhlin, A fast algorithm for particle simulations, Journal of Computational Physics 73 (1987) 325–348.
[4] B.R. Brooks, R.E. Bruccoleri, B.D. Olafson, D.J. States, S. Swaminathan, M. Karplus, CHARMM: a program for macromolecular energy, minimization and dynamic simulation, Journal of Computational Chemistry 4 (2) (1983) 187–217.
[5] Laximikant Kale, Robert Skeel, Minilind Bhandarkar, Robert Brunner, Attila Grusoy, Neal Krawetz, James Phillips, Aritomo Shinozaki, Krishnan Varadarajan, Klaus Schulten, Namd2: greater scalability for parallel molecular dynamics, Journal of Computational Physics 151 (1999) 283–312.
[6] Markus Eichinger, Helmut Heller, Helmut Grubmuller, EGO – An efficient molecular dynamics program and its application to protein dynamics simulations, in: Rudiger Esser, Peter Grassberger, Johannes Grotendorst, Marius Lewerenz (Eds.), Workshop on Molecular Dynamics on Parallel Computers, World Scientific, Singapore, 2000, pp. 154–174.
[7] Philippe Durand, Georges Trinquier, Yves-Henri Sanejouand, A new approach for determining low-frequency normal modes in macromolecules, Biopolymers 34 (1994) 759–771.
[8] Oren M. Becker, Alexander D. MacKerell Jr., Benoit Roux, Masakatsu Watanabe, Computational Biochemistry and Biophysics, Marcel Dekker, Inc., New York, Basel, 2001.
[9] C. Touze, O. Thomas, A. Chaigne, Hardening/softening behavior in nonlinear oscillations of structural systems using non-linear normal modes, Journal of Sound and Vibration 273 (2004) 77–101.
[10] J. Carr, Applications of Centre Manifold Theory, Springer-Verlag, New York, 1981.
[11] S.W. Shaw, C. Pierre, Normal modes for non-linear vibratory systems, Journal of Sound and Vibrations 164 (1) (1993) 85–124.
[12] Nicolas Boivin, Christophe Pierre, Steven W. Shaw, Non-linear normal modes, invariance, and modal dynamics approximations of non-linear systems, Nonlinear Dynamics 8 (1995) 315–346.
[13] A.F. Vakakis, Non-linear normal modes (NNMs) and their applications in vibration theory: an overview, Mechanical Systems and Signal Processing 11 (1) (1997) 3–22.
[14] Steven W. Shaw, Christtophe Pierre, Eric Pesheck, Modal-analysis-based reduced-order models for nonlinear structures-an invariant manifold approach, The Shock and Vibration Digest 31 (1) (1999) 3–16.
[15] Hermann G. Matthies, Marcus Meyer, Nonlinear Galerkin methods for the model reduction of nonlinear dynamical systems, Computers and Structures 81 (2003) 1277–1286.
[16] B.F. Feeny, R. Kappagantu, On the physical interpretation of proper orthogonal modes in vibrations, Journal of Sound and Vibration 211 (4) (1998) 607–616.
[17] B. Racindra, Comments on the physical interpretation of proper orthogonal modes in vibrations, Journal of Sound and Vibration 219 (1) (1999) 189–192.
[18] G. Kerschen, J.C. Golinval, Physical interpretation of the proper orthogonal modes using singular value decomposition, Journal of Sound and Vibration 249 (5) (2002) 849–865.
[19] J.L. Lumley, Atmospheric turbulence and radio wave propagation, Journal of Computational Chemistry 23 (13) (1967) 1236–1243.
[20] M.F.A. Azeez, A.F. Vakakis, Proper orthogonal decomposition (POD) of a class of vibroimpact oscillations, Journal of Sound and Vibration 240 (5) (2001) 859–889.
[21] Sanjay Lall, Petr Krysl, Jerrold E. Marsden, Structure-preserving model reduction for mechanical systems, Physica D 184 (2003) 304–318.
[22] M. Meyer, H.G. Matthies, Efficient model reduction in non-linear dynamics using the Karhunen–Loève expansion and dual-weighted-residual methods, Computational Mechanics 31 (2003) 179–191.
[23] Earl H. Dowell, Kenneth C. Hall, Modeling of fluid–structure interaction, Annual Reviews of Fluid Mechanics 33 (2001) 445–490.
[24] R. Elber, M. Karplus, Multiple conformational states of proteins: a molecular dynamics analysis of myoglobin, Science 235 (4786) (1987) 318–321.
[25] Nobuhiro Go, A theorem on amplitudes of thermal atomic fluctuations in large molecules assuming specific conformations calculated by normal mode analysis, Biophysical Chemistry 35 (1990) 105–112.
[26] Steven Hayward, Akio Kitao, Nobuhiro Go, Harmonic and anharmonic aspects in the dynamics of BPTI: a normal mode analysis and principal component analysis, Protein Science 3 (1994) 936–943.
[27] Steven Hayward, Nobuhiro Go, Collective variable description of native protein dynamics, Annual Review of Physical Chemistry 46 (1995) 223–250.
[28] Bernard R. Brooks, Dusanka Janezic, Martin Karplus, Harmonic analysis of large systems. I. Methodology, Journal of Computational Chemistry 16 (12) (1995) 1522–1542.
[29] Bernard R. Brooks, Dusanka Janezic, Martin Karplus, Harmonic analysis of large systems. II. Comparison of different protein models, Journal of Computational Chemistry 16 (12) (1995) 1543–1553.

[30] Dusanka Janezic, Richard M. Venable, Bernard R. Brooks, Harmonic analysis of large systems. III. Comparison with molecular dynamics, Journal of Computational Chemistry 16 (12) (1995) 1554–1566.
[31] Akio Kitao, Nobuhiro Go, Investigating protein dynamics in collective coordinate space, Current Opinion in Structural Biology 9 (1999) 164–169.
[32] Deman Tang, Aiqin Li, Peter Attar, Earl H. Dowell, Reduced order dynamic model for polysacchrides molecule attached to an atomic force microscope, Journal of Computational Physics 201 (2004) 723–752.
[33] Sookhee N. Ha, Ann Giammona, Martin Field, John W. Brady, A revised potential-energy surface for molecular mechanics studies of carbohydrates, Carbohydrate Research 180 (1988) 207–221.
[34] Michelle Kuttel, J.W. Brady, Kevin J. Brady, Carbohydrate solution simulations: producing a force field with experimentally consistent primary alcohol rotational frequencies and populations, Journal of Computational Chemistry 23 (13) (2001) 1236–1243.
[35] Earl H. Dowell, Deman Tang, Multiscale, multiphenomena modeling and simulation at the nanoscale: on constructing reduced order models for nonlinear dynamical systems with many degrees-of-freedom, Journal of Applied Mechanics 70 (3) (2003) 328–338.
[36] Deman Tang, Earl H. Dowell, Reduced order model analysis for two-dimensional molecular dynamic chain structure attached to an atomic force microscope, Journal of Dynamic Systems, Measurement, and Control 126 (3) (2004) 531–546.
[37] J.E. Jackson, A User's Guide to Principal Components, John Wiley, 1991.
[38] Roy R. Craig Jr., Structural Dynamics: An Introduction to Computer Methods, Wiley, New York, 1981.
[39] Bernard Brooks, Martin Karplus, Harmonic dynamics of proteins: normal modes and fluctuations in bovine pancreatic trypsin inhibitor, Biophysics 80 (1983) 6571–6575.
[40] Nobuhiro Go, Tosiyuki Noguti, Testuo Nishikawa, Dynamics of a small globular protein in terms of low-frequency vibrational modes, Biophysics 80 (1983) 3696–3700.
[41] Akio Kitao, Nobuhiro Go, Conformational dynamics of polypeptides and proteins in the dihedral angle space and in the cartesian coordinate space: normal mode analysis of Deca-Alanine, Journal of Computaional Chemistry 12 (3) (1991) 359–368.